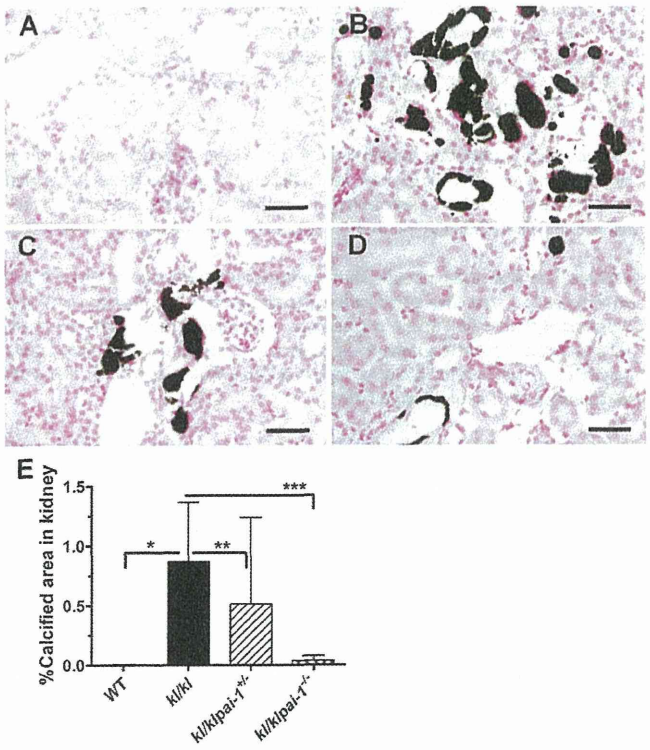

Fig. 5. Effects of PAI-1 deficiency on ectopic calcification characterized by von Kossa staining. Ectopic calcification analysis was performed on kidney ($n = 5$ for each group) sections. Although samples from (*A*) WT mice showed no detectable calcification, kidney sections from (*B*) *kl/kl* mice had remarkable calcified deposits. (*C*) Partial (*kl/klpai-1*$^{+/-}$) or (*D*) complete PAI-1 deficiency (*kl/klpai-1*$^{-/-}$), on the other hand, significantly decreased calcification levels. (Scale bars: 40 μm.) (*E*) Quantitative analyses using Image-Pro-6.3 software showed that the percentages of calcified areas in kidneys were reduced by 41% in *kl/klpai-1*$^{+/-}$ and 96% in *kl/klpai-1*$^{-/-}$ mice compared with *kl/kl* mice. $*P = 0.002$, $**P = 0.03$, and $***P = 0.0001$. Data are plotted as mean ± SD.

senescence in vitro. Because PAI-1 is the main physiological inhibitor of t-PA, IGFBP-3 appears to be a critical downstream target of PAI-1–induced senescence. These findings provide a possible mechanistic explanation for the prosenescent effects of increased PAI-1 in *kl/kl* mice and suggest a role for an extracellular cascade of secreted proteins in the regulation of cellular senescence and physiological aging.

It was recently shown that membrane-bound Klotho prevents the retinoic-acid-inducible gene-I–induced expression of IL-6 and -8 both in vitro and in vivo, suggesting that the antiaging function of Klotho also includes the suppression of inflammation (38). It is interesting to note that with PAI-1 deficiency, levels of both IGFBP-3 and IL-6 were normalized in *kl/kl* mice. This confirms and extends the recent observations by López-Andrés et al. that modulating the activity of a key member of the SMS can also normalize the levels of other SMS factors (39). This indicates that IGFBP-3 and IL-6 are downstream from PAI-1 in the senescence pathway.

In human fibroblasts, telomere shortening initiates senescence through a pathway that involves ataxia telangiectasia mutated (ATM), p53, and p21^{CIP1}, but not p16^{Ink4a} (9). Thus, the presence of p16^{Ink4a}-positive but not p21-positive cells in kidneys of *kl/kl* mice suggests that the pathway to senescence and accelerated aging in the renal tissue of *kl/kl* mice is likely mediated by p16^{Ink4a} and occurs independently of the p53 pathway. These findings in the kidney of preserved telomere length, together with augmented p16^{Ink4a} expression, suggest that renal cells undergo senescence without the requisite cellular division to shorten telomeres (22).

The results presented here indicate that PAI-1 is a critical contributor to, and not merely a marker of, senescence in vivo (12), and that novel therapies targeting PAI-1 or other components of the SMS (40) may prevent senescence and age-related pathologic changes in humans, including arteriosclerosis and emphysema. The development of small-molecule, orally active, selective PAI-1 antagonists, such as TM5441 and others (41), will allow these hypotheses to be tested prospectively.

Materials and Methods

Animals and Animal Care. The original genetic background of *kl/kl* mice, a kind gift from Makoto Kuro-o (Jichi Medial University, Shimotsuke, Tochigi, Japan), was composed of C57BL/6J and C3H/J (13). PAI-1–deficient mice were obtained from The Jackson Laboratory (background strain C57BL/6J; strain name B6.129S2-Serpine1tm1Mlg/J; stock no. 002507). *Klotho* mice and PAI-1–deficient mice were crossed to generate the heterozygous dihybrid mice (*KL/kl-pai-1*$^{+/-}$). All mice used in this study were littermates generated by breeding these *KL/kl-pai-1*$^{+/-}$ mice and thus of the same mixed background. They were housed in a temperature-controlled environment with a daily 14:10 h light–dark cycle and had unlimited access to food (standard rodent chow diet; Harlan Teklad) and water. All experimental protocols were approved by the Institutional Animal Care and Use Committee of Northwestern University.

PAI-1 Inhibitor TM5441. TM5441 was derived from the original hit compound TM5007 (42) and the lead compound TM5275 (43) through an extensive structure-activity relationship (44). We have recently described the pharmacokinetic properties and toxicity, and specificity of TM5441 (20). TM5441 was administered at 100 mg/kg·d^{-1} mixed in the chow.

Histological Methods. Tissues harvested from mice were fixed in formalin for 24–48 h and then processed overnight and embedded in paraffin. Tissues sectioned at 6-μm thickness were stained with Masson's trichrome to visualize tissue morphology. Ectopic calcification was analyzed by von Kossa staining of kidneys ($n = 5$ for each study group). The extent of calcification was quantified in multiple kidney sections from each mouse by using Image-Pro-6.3 image-processing software and the results presented as the percent calcified areas in kidneys (Fig. 3). To detect the senescent cells, tissue sections were immunostained overnight at 4 °C with a primary antibody to p16^{Ink4a} antigen (Cell Applications), and then the antigen was visualized with an HRP-conjugated secondary antibody (goat anti-mouse IgG at 1:500 dilution; Santa Cruz Biotechnology, Inc.). One-Step AEC Solution (BioGenex) was used as the substrate for antigen detection.

Quantitation of Factors in Plasma and Serum. Plasma levels of IGFBP-3, IL-6, and FGF23 were measured using the ELISA kits Quantikine Immunoassay kit from R&D Systems (catalog no. MGB300), Becton-Dickinson (catalog no. 555220), and Immutopics (catalog no. 60-6300), respectively, by following the manufacturers' suggested protocols. Vitamin D_3 levels in plasma were measured using the mouse 1,25-$(OH)_2$VitD3 HVD3 ELISA kit from NovaTein Biosciences (catalog no. NB-E20523). Calcium (catalog no. 0150-250), creatinine (catalog no. 0430-120), and phosphate (catalog no. 0830-125) levels were determined by using kits from Stanbio Laboratories. Plasma PAI-1 levels were measured with the Murine PAI-1 Total Antigen Assay from Molecular Innovations. A colorimetric assay kit and an ELISA kit from Abcam were used to measure serum levels of ALP and aldosterone (catalog nos. ab83369 and ab136933, respectively).

Measuring Partial Oxygen Pressure in Arterial Blood. PaO_2 levels in the arterial blood were measured in mice anesthetized with pentobarbital (75 mg/kg body weight, administered i.p.). After adequate anesthesia was achieved, we performed a tracheostomy and sutured a 20-gauge angiocatheter into the trachea. Mice were then placed on a small rodent ventilator (MiniVent; Harvard Apparatus) with the following settings: a respiratory rate of 150 breaths per minute, a tidal volume of 8 mL/kg body weight, and an FiO_2 of 0.21 (room air) as described previously (45). The animals were ventilated for 15 min before a thoracotomy was performed and then 200 μL arterial blood were collected into a heparinized syringe via direct puncture of the left ventricle. The arterial blood sample was processed for gas analysis using the Stat Profile pHOx blood gas analyzer (Nova Biomedical).

Quantitation of ATLR. Genomic DNA isolated from various tissues was used to measure telomere length by qRT-PCR as previously described with minor modification (46, 47). Briefly, telomere repeats were amplified using specially designed primers, which were then compared with the amplification of

a single-copy gene, the 36B4 gene (acidic ribosomal phosphoprotein PO), to determine the ATLR. One hundred nanograms of genomic DNA template were added to each 20 μL reaction containing forward and reverse primers (250 nM each for telomere primers, and 500 nM each for the 36B4 primers), SsoAdvanced SYBR Green Supermix (Bio-Rad USA), and nuclease-free water. A serially diluted standard curve of 100 ng to 3.125 ng per well of template DNA from a WT mouse sample was included on each plate for both the telomere and the 36B4 reactions to facilitate ATLR calculation. Critical values were converted to nanogram values according to the standard curves, and nanogram values of the telomere (T) reaction were divided by the nanogram values of the 36B4 (S) reaction to yield the ATLR. The primer sequences for the telomere portion were as follows: 5′-CGG TTT GTT TGG GTT TGG GTT TGG GTT TGG GTT TGG GTT-3′ and 5′-GGC TTG CCT TAC CCT TAC CCT TAC CCT TAC CCT TAC CCT-3′. The primer sequences for the 36B4 single copy gene portion were as follows: 5′-ACT GGT CTA GGA CCC GAG AAG-3′ and 5′-TCA ATG GTG CCT CTG GAG ATT-3′. Cycling conditions for both primer sets (run in the same plate) were 95 °C for 10 min, 30 cycles of 95 °C for 15 s, and 55 °C for 1 min for annealing and extension.

qRT-PCR. Tissues harvested from subject mice were snap-frozen in liquid nitrogen. Excess tissue was removed under a dissecting microscope. RNA was isolated using the Qiagen RNAeasy Mini Kit (Qiagen) using the manufacturer's protocol. cDNA was generated from the RNA using the qScript cDNA Supermix (Quanta Biosciences). qRT-PCR was performed using the SsoAdvanced SYBR Green Supermix (Bio-Rad USA). Forward and reverse primers used for $p16^{Ink4a}$ expression were, respectively: 5′-AGGGCCGTGTGCATGACGTG-3′ and 5′-GCACCGGGCGGGAGAAGGTA-3′; for PAI-1 expression, respectively: 5′-ACGCCTGGTGCTGGTGAATGC-3′ and 5′-ACGGTGCTGCCATCAGACTTGTG-3′; and for GAPDH expression, respectively: 5′-ATGTTCCAGTATGACTCCACTCACG-3′ and 5′-GAAGACACCAGTAGACTCCACGACA-3′ (IDT, Inc.).

Behavioral Characterization. To test the effect of PAI-1 deficiency on the level of physical activity of *kl/kl* mice, the open field test for spontaneous horizontal activity was performed on age-matched animals at the Northwestern University Mouse Behavioral Phenotyping Core Laboratory as described previously (13).

Statistical Analyses. We present the averaged values obtained for each study as mean ± SD. Statistical significance was assigned to a comparison by using an unpaired, two-tailed Student *t* test when comparing two groups. Statistical significance for the survival of groups was established by the log-rank analysis of Kaplan–Meier plots using GraphPad Prism 4 software. $P < 0.05$ was considered statistically significant.

ACKNOWLEDGMENTS. We thank Dr. Makoto Kuro-o for providing us with the *kl/kl* mice. We also thank Marissa Michaels for her help in obtaining reagents and coordinating various aspects of our projects. This work was supported by National Institutes of Health (NIH)/National Heart, Lung, and Blood Institute Grants 2R01HL051387 and 1P01HL108795. A.T.P. is supported in part by NIH National Institute of Diabetes and Digestive and Kidney Diseases Training Grant T32 KD007169.

1. Rodier F, Campisi J (2011) Four faces of cellular senescence. *J Cell Biol* 192(4):547–556.
2. Campisi J, d'Adda di Fagagna F (2007) Cellular senescence: When bad things happen to good cells. *Nat Rev Mol Cell Biol* 8(9):729–740.
3. Coppé JP, Desprez PY, Krtolica A, Campisi J (2010) The senescence-associated secretory phenotype: The dark side of tumor suppression. *Annu Rev Pathol* 5:99–118.
4. Krtolica A, Parrinello S, Lockett S, Desprez PY, Campisi J (2001) Senescent fibroblasts promote epithelial cell growth and tumorigenesis: A link between cancer and aging. *Proc Natl Acad Sci USA* 98(21):12072–12077.
5. Mu XC, Higgins PJ (1995) Differential growth state-dependent regulation of plasminogen activator inhibitor type-1 expression in senescent IMR-90 human diploid fibroblasts. *J Cell Physiol* 165(3):647–657.
6. Kuilman T, Peeper DS (2009) Senescence-messaging secretome: SMS-ing cellular stress. *Nat Rev Cancer* 9(2):81–94.
7. Dimri GP, et al. (1995) A biomarker that identifies senescent human cells in culture and in aging skin in vivo. *Proc Natl Acad Sci USA* 92(20):9363–9367.
8. Wahl GM, Carr AM (2001) The evolution of diverse biological responses to DNA damage: Insights from yeast and p53. *Nat Cell Biol* 3(12):E277–E286.
9. Herbig U, Jobling WA, Chen BP, Chen DJ, Sedivy JM (2004) Telomere shortening triggers senescence of human cells through a pathway involving ATM, p53, and p21 (CIP1), but not p16(INK4a). *Mol Cell* 14(4):501–513.
10. Serrano M, Lin AW, McCurrach ME, Beach D, Lowe SW (1997) Oncogenic ras provokes premature cell senescence associated with accumulation of p53 and p16INK4a. *Cell* 88(5):593–602.
11. Parrinello S, et al. (2003) Oxygen sensitivity severely limits the replicative lifespan of murine fibroblasts. *Nat Cell Biol* 5(8):741–747.
12. Baker DJ, et al. (2011) Clearance of p16Ink4a-positive senescent cells delays ageing-associated disorders. *Nature* 479(7372):232–236.
13. Kuro-o M, et al. (1997) Mutation of the mouse klotho gene leads to a syndrome resembling ageing. *Nature* 390(6655):45–51.
14. Baker DJ, et al. (2008) Opposing roles for p16Ink4a and p19Arf in senescence and ageing caused by BubR1 insufficiency. *Nat Cell Biol* 10(7):825–836.
15. Liu H, et al. (2007) Augmented Wnt signaling in a mammalian model of accelerated aging. *Science* 317(5839):803–806.
16. Doi S, et al. (2011) Klotho inhibits transforming growth factor-beta1 (TGF-beta1) signaling and suppresses renal fibrosis and cancer metastasis in mice. *J Biol Chem* 286(10):8655–8665.
17. Kurosu H, et al. (2005) Suppression of aging in mice by the hormone Klotho. *Science* 309(5742):1829–1833.
18. Takeshita K, et al. (2002) Increased expression of plasminogen activator inhibitor-1 with fibrin deposition in a murine model of aging, "Klotho" mouse. *Semin Thromb Hemost* 28(6):545–554.
19. Kortlever RM, Higgins PJ, Bernards R (2006) Plasminogen activator inhibitor-1 is a critical downstream target of p53 in the induction of replicative senescence. *Nat Cell Biol* 8(8):877–884.
20. Boe AE, et al. (2013) Plasminogen activator inhibitor-1 antagonist TM5441 attenuates Nω-nitro-L-arginine methyl ester-induced hypertension and vascular senescence. *Circulation* 128(21):2318–2324.
21. Morishita K, et al. (2001) The progression of aging in klotho mutant mice can be modified by dietary phosphorus and zinc. *J Nutr* 131(12):3182–3188.
22. Coviello-McLaughlin GM, Prowse KR (1997) Telomere length regulation during postnatal development and ageing in Mus spretus. *Nucleic Acids Res* 25(15):3051–3058.
23. Suga T, et al. (2000) Disruption of the klotho gene causes pulmonary emphysema in mice. Defect in maintenance of pulmonary integrity during postnatal life. *Am J Respir Cell Mol Biol* 22(1):26–33.
24. Voelkl J, et al. (2013) Spironolactone ameliorates PIT1-dependent vascular osteoinduction in klotho-hypomorphic mice. *J Clin Invest* 123(2):812–822.
25. Fischer SS, et al. (2010) Hyperaldosteronism in Klotho-deficient mice. *Am J Physiol Renal Physiol* 299(5):F1171–F1177.
26. Eren M, Painter CA, Atkinson JB, Declerck PJ, Vaughan DE (2002) Age-dependent spontaneous coronary arterial thrombosis in transgenic mice that express a stable form of human plasminogen activator inhibitor-1. *Circulation* 106(4):491–496.
27. Bernot D, et al. (2011) Plasminogen activator inhibitor 1 is an intracellular inhibitor of furin proprotein convertase. *J Cell Sci* 124(Pt 8):1224–1230.
28. Fukumoto S (2005) Post-translational modification of Fibroblast Growth Factor 23. *Ther Apher Dial* 9(4):319–322.
29. Thomas G (2002) Furin at the cutting edge: From protein traffic to embryogenesis and disease. *Nat Rev Mol Cell Biol* 3(10):753–766.
30. Tian S, Huang Q, Fang Y, Wu J (2011) FurinDB: A Database of 20-Residue Furin Cleavage Site Motifs, Substrates and Their Associated Drugs. *Int J Mol Sci* 12(2):1060–1065.
31. Razzaque MS (2009) The FGF23-Klotho axis: Endocrine regulation of phosphate homeostasis. *Nat Rev Endocrinol* 5(11):611–619.
32. Yamamoto M, et al. (2005) Regulation of oxidative stress by the anti-aging hormone klotho. *J Biol Chem* 280(45):38029–38034.
33. Hu MC, et al. (2011) Klotho deficiency causes vascular calcification in chronic kidney disease. *J Am Soc Nephrol* 22(1):124–136.
34. Ohnishi M, Nakatani T, Lanske B, Razzaque MS (2009) Reversal of mineral ion homeostasis and soft-tissue calcification of klotho knockout mice by deletion of vitamin D 1alpha-hydroxylase. *Kidney Int* 75(11):1166–1172.
35. Lim K, et al. (2012) Vascular Klotho deficiency potentiates the development of human artery calcification and mediates resistance to fibroblast growth factor 23. *Circulation* 125(18):2243–2255.
36. Brown NJ, et al. (2000) Aldosterone modulates plasminogen activator inhibitor-1 and glomerulosclerosis in vivo. *Kidney Int* 58(3):1219–1227.
37. Elzi DJ, et al. (2012) Plasminogen activator inhibitor 1—insulin-like growth factor binding protein 3 cascade regulates stress-induced senescence. *Proc Natl Acad Sci USA* 109(30):12052–12057.
38. Liu F, Wu S, Ren H, Gu J (2011) Klotho suppresses RIG-I-mediated senescence-associated inflammation. *Nat Cell Biol* 13(3):254–262.
39. López-Andrés N, et al. (2013) Absence of cardiotrophin 1 is associated with decreased age-dependent arterial stiffness and increased longevity in mice. *Hypertension* 61(1):120–129.
40. Peeper DS (2011) Ageing: Old cells under attack. *Nature* 479(7372):186–187.
41. Tashiro Y, et al. (2012) Inhibition of PAI-1 induces neutrophil-driven neoangiogenesis and promotes tissue regeneration via production of angiocrine factors in mice. *Blood* 119(26):6382–6393.
42. Izuhara Y, et al. (2008) Inhibition of plasminogen activator inhibitor-1: Its mechanism and effectiveness on coagulation and fibrosis. *Arterioscler Thromb Vasc Biol* 28(4):672–677.
43. Izuhara Y, et al. (2010) A novel inhibitor of plasminogen activator inhibitor-1 provides antithrombotic benefits devoid of bleeding effect in nonhuman primates. *J Cereb Blood Flow Metab* 30(5):904–912.
44. Miyata T, Yamaoka N, Kodama H, Murano K (2011) Inhibitor of plasminogen activator inhibitor-1. US Patent Appl 2,011,112,140 A1 (May 12, 2011).
45. Mutlu GM, et al. (2004) Upregulation of alveolar epithelial active Na+ transport is dependent on beta2-adrenergic receptor signaling. *Circ Res* 94(8):1091–1100.
46. Cawthon RM (2002) Telomere measurement by quantitative PCR. *Nucleic Acids Res* 30(10):e47.
47. Callicott RJ, Womack JE (2006) Real-time PCR assay for measurement of mouse telomeres. *Comp Med* 56(1):17–22.

STEM CELLS®

TISSUE-SPECIFIC STEM CELLS

Inhibition of Plasminogen Activator Inhibitor Type-1 Activity Enhances Rapid and Sustainable Hematopoietic Regeneration

ABD AZIZ IBRAHIM,[a,b] TAKASHI YAHATA,[a,c] MAKOTO ONIZUKA,[a,b] TAKASHI DAN,[d] CHARLES VAN YPERSELE DE STRIHOU,[e] TOSHIO MIYATA,[d] KIYOSHI ANDO[a,b]

Key Words. Hematopoietic stem cells • Bone marrow stromal cells • Hematopoiesis • Stem cell transplantation • Tissue regeneration • Osteoblast

[a]Division of Hematopoiesis, Research Center for Regenerative Medicine, [b]Department of Hematology and Oncology, [c]Department of Cell Transplantation and Regenerative Medicine; Tokai University School of Medicine, Isehara, Kanagawa, Japan; [d]Molecular Medicine and Therapy, United Centers for Advanced Research and Translational Medicine, Tohoku University Graduate School of Medicine, Sendai, Miyagi, Japan; [e]Service de Nephrologie, Universite Catholique de Louvain, Brussels, Belgium

Correspondence: Takashi Yahata, Ph.D., Tokai University School of Medicine, Isehara, Kanagawa 259-1193, Japan. Telephone: 81-463-1121; Fax: 81-463-92-4750; e-mail: yahata@is.icc.u-tokai.ac.jp; or Kiyoshi Ando, M.D., Ph.D., Tokai University School of Medicine, Isehara, Kanagawa 259-1193, Japan. Telephone: 81-463-1121; Fax: 81–463-92-4750; e-mail: andok@keyaki.cc.u-tokai.ac.jp

Received August 12, 2013; accepted for publication October 3, 2013; first published online in STEM CELLS *EXPRESS* October 24, 2013.

1066-5099/2014/$30.00/0

http://dx.doi.org/10.1002/stem.1577

ABSTRACT

The prognosis of patients undergoing hematopoietic stem cell transplantation (HSCT) depends on the rapid recovery and sustained life-long hematopoiesis. The activation of the fibrinolytic pathway promotes hematopoietic regeneration; however, the role of plasminogen activator inhibitor-1 (PAI-1), a negative regulator of the fibrinolytic pathway, has not yet been elucidated. We herein demonstrate that bone marrow (BM) stromal cells, especially osteoblasts, produce PAI-1 in response to myeloablation, which negatively regulates the hematopoietic regeneration in the BM microenvironment. Total body irradiation in mice dramatically increased the local expression levels of fibrinolytic factors, including tissue-type plasminogen activator (tPA), plasmin, and PAI-1. Genetic disruption of the *PAI-1* gene, or pharmacological inhibition of PAI-1 activity, significantly improved the myeloablation-related mortality and promoted rapid hematopoietic recovery after HSCT through the induction of hematopoiesis-promoting factors. The ability of a PAI-1 inhibitor to enhance hematopoietic regeneration was abolished when *tPA*-deficient mice were used as recipients, thus indicating that PAI-1 represses tPA-dependent hematopoietic regeneration. The PAI-1 inhibitor not only accelerated the expansion of the donor HSCs during the early-stage of regeneration, but also supported long-term hematopoiesis. Our results indicate that the inhibition of PAI-1 activity could be a therapeutic approach to facilitate the rapid recovery and sustained hematopoiesis after HSCT. STEM CELLS *2014;32:946–958*

INTRODUCTION

Hematopoietic stem cell transplantation (HSCT) is used as a therapy for patients who suffer from hematological malignancies. In general, such patients are myeloablated by chemotherapy and/or radiotherapy to eradicate the deranged host hematopoietic system, followed by transplantation of healthy donor-derived hematopoietic cells [1]. However, due to a low engraftment efficiency and delayed bone marrow (BM) reconstitution, these patients occasionally suffer from severe immunodeficiency, thus leading to an increased susceptibility to serious infectious diseases, and therefore, to a high-risk of transplant-related death [2]. The establishment of an efficient strategy to improve the recovery and sustain hematopoiesis is a goal in the treatment of patients undergoing HSCT.

The fibrinolytic pathway breaks down fibrin clots in the blood, and plasmin plays a central role in this process [3]. The proenzyme plasminogen (Plg) is produced from the liver and circulates in the blood stream. Under certain circumstances, such as wound healing, Plg is proteolytically converted into the active enzyme plasmin by tissue-type plasminogen activator (tPA), which is released from endothelial cells [4]. The blood also contains negative regulators of the fibrinolysis pathway, including plasminogen activator inhibitor-1 (PAI-1). The production of plasmin from plasminogen is thus regulated by a balance between activator molecules (e.g., tPA) and their inhibitors (e.g., PAI-1) [4, 5]. Therefore, inhibiting the PAI-1 activity is expected to accelerate the activation of the tPA-mediated fibrinolytic pathway.

Recently, Hattori and colleagues demonstrated that the fibrinolytic pathway regulates hematopoietic regeneration [6, 7]. They showed that the deletion of the Plg gene impaired the entry of quiescent HSCs into the cell cycle and delayed hematopoietic regeneration. In contrast, the activation of Plg by the exogenous administration of recombinant tPA promoted HSC proliferation and differentiation

through the potentiation of matrix metalloproteinase (MMP)-mediated release of c-kit ligand (c-kitL) from BM stromal cells. The fibrinolytic pathway thus plays a role in hematopoiesis.

We have recently developed a low molecular weight synthetic inhibitor of PAI-1, TM5275 (5-chloro-2[[(2-[4-(diphenylmethyl) piperazine-1yl]-2-oxoethoxy)acetyl) amino]benzoate) [8, 9]. TM5275 binds selectively to the A β-sheet (s4A) position of the PAI-1 molecule, preventing the formation of the PAI-1/tPA complex, thereby preserving active tPA. Previous studies have demonstrated that TM5275, which was given orally, provided antithrombotic benefits without prolonging the bleeding time in rodent and monkey thrombosis models [10]. Given the potential importance of the fibrinolytic pathway in HSCT, in this study, we addressed whether the suppression of PAI-1 activity could affect the hematopoietic regeneration after transplantation in PAI-1 knockout (KO) mice and using the PAI-1 inhibitor, TM5275. Our study demonstrates that PAI-1 is a negative regulator of hematopoietic regeneration, and that suppression of the PAI-1 activity leads to both a rapid recovery and long-term maintenance of donor-derived hematopoiesis. Therefore, the inhibition of PAI-1 activity could be a therapeutic approach to facilitate rapid recovery and sustained hematopoiesis.

Materials and Methods

Animals

Eight- to twelve-week-old C57Bl/6J mice were purchased from CLEA Japan (Tokyo, Japan, www.clea-japan.com). *PAI-1*-deficient mice (B6.12952-Serpine1^{tm1Mg}/J) [11, 12] were purchased from Jackson Laboratory (Bar Harbor, ME, www.jax.org). *tPA*-deficient mice (B6.129S2-Plat^{tm1Mlg}/J) [13] were kindly provided by Dr. Koichi Hattori, University of Tokyo, Japan. All mice were housed in cages at the animal facility of Tokai University School of Medicine. All the protocols for animal experiments were approved by the Animal Care Committee of Tokai University, and animals were treated in accordance with the institutional guidelines.

Cell Transplantation

To distinguish donor (Ly5.1)- and recipient (Ly5.2)-derived BM cells, we used the Ly5.1/Ly5.2 congenic system and analyzed the reconstitution of hematopoietic cells by a fluorescence-activated cell sorting (FACS) analysis by gating Ly5.1$^+$ donor-derived cells. Before transplantation, the recipient mice were lethally irradiated (9 Gy) in an x-ray irradiator (MBR-1520R-3, Hitachi Medico, Tokyo, Japan, www.hitachi-power-solution.com). Ly5.1$^+$ BM mononucleic cells (MNCs, 2.5 $\times$ 10^6) were transplanted intravenously into the retro-orbital plexus of Ly5.2$^+$ congenic mice.

For the secondary transplantation, 1 $\times$ 10^6 donor-derived Ly5.1$^+$ BM MNCs from the primary recipients were retransplanted into Ly5.2$^+$ secondary recipients which had been irradiated with 9 Gy. To protect secondary recipients from radiation-related lethality, 5 $\times$ 10^5 Ly5.2$^+$ competitor cells were transplanted along with the Ly5.1$^+$ donor cells. To compare the proportion of long-term HSCs, Ly5.1$^+$ BM cells from the primary recipients were serially diluted and administered along with 5 $\times$ 10^5 Ly5.2$^+$ competitor cells into secondary recipients that had been irradiated with 9 Gy. At 12 weeks after secondary transplantation, the BM MNCs were collected and stained with APC-conjugated anti-Ly5.1, FITC-conjugated anti-B220, PE-conjugated anti-Gr-1 and anti-Mac-1 antibodies, and were analyzed by FACS LSRFortessa (BD Bioscience, San Jose, CA, www.bdbioscience.com). The proportion of donor cells was calculated from a total of 200,000 events. Successfully engrafted mice were defined as recipients that contained more than 1.0% Ly5.1$^+$ donor-derived cells with both lymphoid (B220$^+$) and myeloid (Gr-1$^+$/Mac-1$^+$) differentiation markers. In the radioprotection assay, we used 12 Gy irradiation, which results in 20% survival when 1 $\times$ 10^6 cells were transplanted (Supporting Information Fig. S1).

Administration of the PAI-1 Inhibitor or tPA

TM5275 is a specific inhibitor of PAI-1 molecules that had a half-maximal inhibition (IC_{50}) value of 6.95 μM in a tPA-dependent hydrolysis assay [8, 10]. It does not interfere with other serpin/serine protease systems, such as the alpha1-antitrypsin/trypsin and alpha2-antiplasmin/plasmin systems.

After BM transplantation, TM5275 (100 mg/kg) or vehicle (saline) was administered daily to mice via oral gavage using a feeding needle for 5 consecutive days. Recombinant tPA (10 mg/kg, Eisai, Tokyo, Japan, www.eisai.com) was administered to the mice daily by intraperitoneal injection for 5 consecutive days. The dosage is equivalent to that used in the clinical setting.

Immunohistochemistry

Isofluorane-anesthetized mice were perfused with 4% paraformaldehyde in phosphate buffered saline (PBS) through the left ventricle. The femur and tibia were removed, decalcified, embedded in OCT compound, and frozen in liquid nitrogen. Alternatively, the decalcified bones were embedded in paraffin. The deparaffinized sections were stained for tPA by incubation with a rabbit anti-mouse tPA polyclonal antibody (Santa Cruz Biotechnology, California, CA, www.scbt.com), for Plg/plasmin with a rabbit anti-human Plg/plasmin polyclonal antibody (Santa Cruz Biotechnology) or for PAI-1 with a rabbit anti-mouse PAI-1 polyclonal antibody (Abcam, Cambridge, MA, www.abcam.com), followed by visualization with a catalyzed signal amplification II system (Dako, California, CA, www.dako.com). The slides were then developed with diaminobenzidine and counterstained with methyl green. For the double immunohistochemical staining analysis, the bone sections were stained with PAI-1 or tPA antibodies, followed by costaining with either rat anti-mouse PECAM-1 (CD31) monoclonal antibodies (BD BioSciences), goat anti-mouse osteocalcin polyclonal antibodies (Santa Cruz Biotechnology), or goat anti-mouse alpha one chain of type I collagen (Col(I) α1) polyclonal antibodies (Santa Cruz Biotechnology). Serial sections of bone were stained with rabbit anti-mouse c-kit polyclonal antibodies (Santa Cruz Biotechnology) or rabbit anti-mouse proliferation cell nuclear antigen (PCNA) polyclonal antibodies (Abcam). Fluorescent immunohistochemistry was also performed with secondary antibodies as follows: Alexa Fluor 488 goat anti-rabbit IgG, Alexa Fluor 594 donkey anti-goat IgG or Alexa Fluor 594 goat anti-rabbit IgG secondary antibody (Life Technologies Corporation, Grand Island, NY, www.lifetechnologies.com), followed by counterstaining with 4′,6-diamidino-2-phenylindole. The endosteal region of the BM was defined as that within 12 cells from the endosteum [14, 15]. Images were captured using a HS All-in-one Fluorescence Microscope Biorevo 9000 (Keyence Corporation, Osaka, Japan, www.keyence.com) and analyzed by the BZ II analyzer software program (Keyence Corporation).

Evaluation of the tPA, Plasmin, PAI-1, MMP-9, and C-KitL Levels in Blood Plasma and BM Fluid

Plasma was prepared from peripheral blood (PB) with EDTA as an anticoagulant, and then the specimens were centrifuged at 11,600*g* for 10 minutes to completely remove platelets. BM liquid was collected as described previously [16]. Briefly, four long leg bones were perused with 1 ml of PBS containing 2 mM ethylenediaminetetraacetic acid (EDTA) and 0.5% bovine serum albumin (BSA). BM cells were removed by centrifugation at 350*g*, and the resulting supernatant was designated as BM liquid. The volume of the BM cavities of the bones was assumed to be 25 μl in this study, and the cytokines concentration were multiplied by this dilution factor (1,000/25 = 40×) and expressed per unit BM volume as described previously [16]. The concentrations of plasmin (Innovative Research, Novi, MI, www.innov-research.com), tPA (Innovative Research), active PAI-1 (Innovative Research), total MMP-9 (R&D System, MN, www.rndsystems.com), and stem cell factor (SCF) (c-kitL, R&D System) in the plasma and in BM fluid were determined by enzyme-linked immunoabsorbent assay (ELISA) kits according to the manufacturers' instructions.

PB Cell Counts

PB was collected and a complete blood count was determined using a Sysmex Hematology Analyzer (Sysmex Co., Kobe, Japan, www.sysmex.com).

Analysis of HSC and Cell Engraftment

On day 2 and 1, 3, and 15 weeks after the infusion of MNCs, the mice were euthanized, and the BM MNCs were collected from the femurs and tibiae. The BM MNCs were counted, and aliquots of cells were stained with various antibodies as noted below. Donor-derived hematopoietic cells were labeled with a PE-conjugated anti-Ly5.1 antibody (CD45.1, BD Biosciences) and biotin-conjugated antibody cocktail for lineage markers (CD5, CD11b, CD45R, Gr-1, 7-4, and Ter119; Miltenyi Biotec, Bergisch Gladbach, Germany, www.miltenyibiotec.com), followed by perinidin chlorophyll protein-cyanine 5.5 (PerCP-Cy5.5)-conjugated streptavidin (BD Biosciences). The labeled cells were divided into two aliquots, each of which was then mixed with either antibody cocktail A (APC-conjugated anti-mouse c-kit [CD117] antibody [eBioscience, San Diego, CA, www.ebioscience.com], PE-Cy7-conjugated anti-mouse Sca-1 [Ly6A/E] antibody [eBioscience], and FITC-conjugated anti-mouse CD34 antibody [eBioscience]) or with antibody cocktail B (APC-conjugated anti-mouse CD48 antibody [eBioscience] and PE-Cy7-conjugated anti-mouse CD150 antibody [eBioscience]). A flow cytometric analysis was performed on the FACS LSRFortessa (BD Bioscience) instruments using the FACS-Diva software program (BD Bioscience). Dead cells were gated out by staining with propidium iodide. The proportion of each lineage was calculated from 1,000,000 events.

Cell Proliferation and Cell Cycle Analysis

At 1 week post-transplantation, Ly5.1$^+$, lineage-negative, Sca-1-positive, c-kit-positive (LSK) cells were isolated and stained with anti-Ki67-FITC antibody according to the manufacturer's instructions (BD Bioscience).

Statistical Analysis

The data were analyzed using unpaired two-tailed Student's *t* tests or the Log-rank test for the survival analysis using the PRISM software program (GraphPad software, LA Jolla, CA, www.graphpad.com). For comparisons of more than three groups, a one-way ANOVA followed by Bonferroni post-tests was performed. A value of $p < .05$ was considered to be significant.

Results

Irradiation Activates the Fibrinolytic Pathway and Increases the Expression of PAI-1 in the BM Microenvironment

To examine the effects of irradiation on the fibrinolytic system in the BM microenvironment, the levels of fibrinolytic factors, such as tPA, plasmin/Plg, and its inhibitor, PAI-1, in the BM fluid and in plasma were measured by ELISA. Two days after 9 Gy irradiation, the levels of tPA and plasmin in the BM fluid, as well as in the plasma, were significantly elevated (Fig. 1A). The level of active PAI-1, a negative regulator of the fibrinolytic system, was also elevated in the plasma and BM fluid of the irradiated mice (Fig. 1A). Of note, the increases of these fibrinolytic factors and PAI-1 were much more prominent in the BM fluid than in the blood, suggesting that the irradiation dramatically activates the fibrinolytic pathway and its inhibitor, PAI-1, in the hematopoietic microenvironment.

Increases in the expression levels of tPA, plasmin (or Plg), and PAI-1 in the BM microenvironment were also confirmed by means of immunohistochemical approaches (Fig. 1B, 1C). The irradiation severely destroyed the BM structure, which may have increased the chance of non-specific staining. Therefore, the specificity of the antibodies used in these immunostaining was verified in tPA KO mice or PAI-1 KO mice. No substantial material in the tissue was stained with the respective antibodies under the same assay conditions in these mice (Supporting Information Fig. S2).

Next, the cells responsible for producing the fibrinolytic factors and PAI-1 in the irradiated BM were identified. tPA was detected in vasculature-lining CD31$^+$ endothelial cells and was significantly elevated after irradiation (Fig. 1B, 1C and Supporting Information Fig. S3A). In agreement with previous reports [4, 5], PAI-1 was detected in megakaryocyte-like cells in untreated mice, but after irradiation, the PAI-1 producing megakaryocyte-like cells disappeared, and the PAI-1 levels in the endosteal region were increased. The tissue distributions of plasmin and Plg colocalized with that of PAI-1 after irradiation (Fig. 1B). Our subsequent double-staining studies revealed that the majority of PAI-1-expressing cells in the irradiated BM were both osteocalcin-positive and Col(I) α1-positive osteoblasts (Fig. 1C and Supporting Information Fig. S3B, S3C).

The activation of fibrinolytic factors and the fibrinolysis inhibitor, PAI-1, in nonhematopoietic cells in the hematopoietic niche shortly after irradiation was also conformed in in vitro studies. We observed that primary BM stromal cells, as well as the BM stromal cell line, HESS5, produced fibrinolytic factors and PAI-1 after irradiation (Fig. 1D and Supporting Information Fig. S4).

PAI-1 Is a Negative Regulator of Early-Phase Hematopoietic Regeneration

To investigate role of PAI-1 in the hematopoietic regeneration, we transplanted 2.5 × 10^6 Ly5.1$^+$ BM MNCs into Ly5.2$^+$

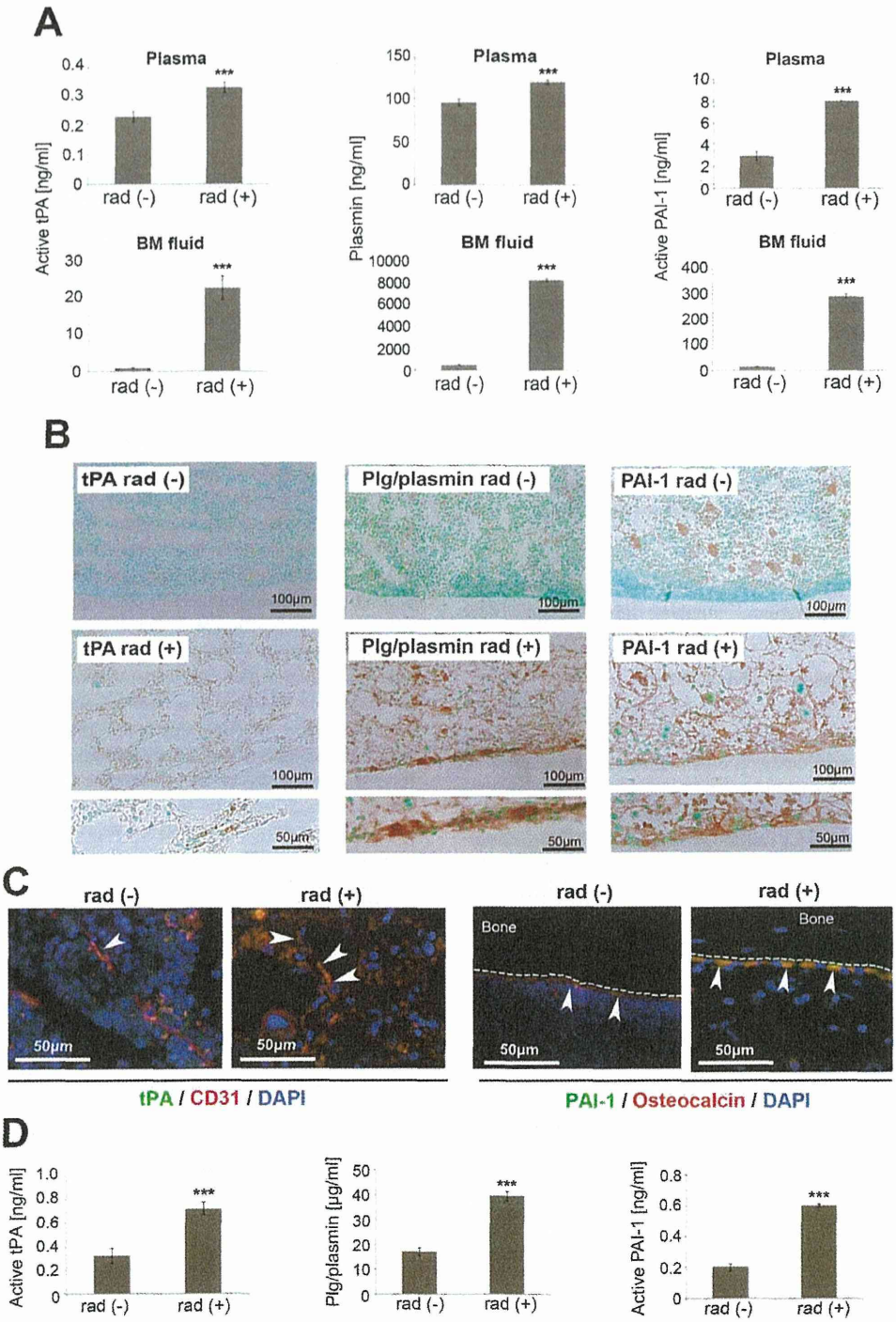

Figure 1. The fibrinolytic pathway and its inhibitor are activated after irradiation. Mice were treated with 9 Gy irradiation [rad (+)] or were untreated [rad (−)], and plasma and BM fluid were collected 2 days later. **(A):** The concentrations of active tPA, plasmin, and active PAI-1 in the plasma and BM fluid were determined by enzyme-linked immunoabsorbent assay (ELISA). Data from three independent experiments are shown ($n = 6$ for each condition; ***, $p < .001$) and are expressed as the means ± SD. **(B, C):** Representative images of immunohistochemical staining for tPA, Plg/plasmin, and PAI-1 in the femur BM. Cells at the endosteal region were intensely stained. (C): The sections were double-immunostained with antibodies for CD31 (red) and tPA (green) (left set), or osteocalcin (red) and PAI-1 (green) (right set). Nuclei were counterstained with DAPI (blue). Arrowheads indicate positive cells. **(D):** The irradiation-induced expression of fibrinolytic factors in cultured BM cells. Primary BM stromal cells in culture were exposed to 10 Gy irradiation. The culture media were collected 24 hours after irradiation, and the concentrations of active tPA, Plg/plasmin, and active PAI-1 were measured by ELISA. Data from three independent experiments are shown ($n = 6$ for each condition; ***, $p < .001$ vs. [rad (−)]) and are expressed as the means ± SD. Abbreviations: BM, bone marrow; DAPI, 4′,6-diamidino-2-phenylindole; PAI-1, plasminogen activator inhibitor-1; tPA, tissue-type plasminogen activator; Plg, plasminogen.

congenic mice, which had been myeloablated by 9 Gy irradiation. PAI-1 KO mice (Ly5.2$^+$) were used as HSCT recipients to monitor the effects of the PAI-1 inhibition on hematopoietic regeneration. The PAI-1 KO recipient mice did not exhibit the induction of active PAI-1, regardless of the transfer of wild-type (WT; PAI-1$^{+/+}$) hematopoietic cells, suggesting that donor-derived hematopoietic cells may not be involved in the regulation of the fibrinolytic pathway during hematopoietic regeneration (Fig. 2A).

A previous study by another group [6] reported that the activation of the fibrinolytic pathway by recombinant tPA promoted hematopoietic cell proliferation through the MMP-mediated release of c-kitL. We therefore evaluated the expression levels of active tPA and other hematopoietic regulatory factors (i.e., MMP-9 and c-kitL) in the PAI-1 KO mice. The results demonstrated a marked increase in the expression of these factors compared to the WT mice at each time point (Fig. 2B–2E).

We subsequently examined the efficiency of hematopoietic regeneration by a flow cytometric analysis (Supporting Information Fig. S5). Over 90% (93.96% $\pm$ 1.56%, $n = 36$) of the hematopoietic cells in the recipient BM were Ly5.1$^+$ donor-derived cells. The absolute number of BM MNCs (Fig. 2F) and the proportion of Ly5.1$^+$ donor-derived Lin$^-$ SLAM (CD150$^+$CD48$^-$) HSCs (Fig. 2G, 2H) were higher in the PAI-1 KO mice than in the WT mice during both the steady state and post-transplant periods. We also examined another HSC marker, CD34$^-$LSK (Lin$^-$Sca-1$^+$c-kit$^+$), and showed that the proportion of Ly5.1$^+$ CD34$^-$LSK cells was higher in the PAI-1 KO mice than in the WT mice (Fig. 2I, 2J), supporting our hypothesis that the induction of PAI-1 in the hematopoietic microenvironment inhibits hematopoietic regeneration. Collectively, our results demonstrated that radiation-induced myeloablation augments the expression levels of not only hematopoietic regeneration-enhancing factors, tPA and Plg/plasmin, but also simultaneously enhances the expression of their negative regulator, PAI-1.

The Expression of Fibrinolytic Factors Is Augmented by PAI-1 Inhibition During Hematopoietic Recovery

We tested our hypothesis that the pharmacological inhibition of PAI-1 can augment the endogenous tPA-mediated fibrinolytic pathway activity more efficiently than exogenous tPA administration, leading to more efficient hematopoietic reconstitution after BM transplantation. A PAI-1 inhibitor or recombinant tPA was thus administered to the WT irradiated mice, and the early phase of hematopoietic recovery and the changes in fibrinolytic factors and the fibrinolysis inhibitor in the plasma were monitored at several time points. The administration of a PAI-1 inhibitor resulted in almost complete suppression of the elevation of active PAI-1 after BM transplantation (Fig. 3A). The PAI-1 inhibitor significantly increased the plasma levels of active tPA and plasmin (Fig. 3B, 3C). Based on the fact that the half-life of recombinant tPA is only a few minutes in rodents [17], as well as the results in Figure 1, it is likely that the increased tPA present at 2 and 7 days post-transplantation reflects the local production of tPA in the BM generated by irradiation. Surprisingly, the PAI-1 inhibitor augmented the induction of fibrinolytic factors more strongly than did the direct administration of recombinant tPA. This may be explained, at least in part, by the fact high PAI-1 activity was maintained during recombinant tPA administration (Fig. 3A), which may limit its benefit on fibrinolytic factors.

We confirmed that administering a PAI-1 inhibitor to mice induced an increase in the plasma levels of hematopoiesis-promoting factors, such as MMP-9 and c-kitL (3- and 1.7-fold compared to the vehicle treatment, respectively) as shown in Figure 3D and 3E. These results demonstrate that the inhibition of PAI-1 effectively induces factors promoting hematopoiesis.

The Activation of the Fibrinolytic Pathway by PAI-1 Inhibition Enhances the Hematopoietic Reconstitution

The protection against BM damage after irradiation and/or chemotherapy is a primary factor that determines the survival rate of animals [18], which hinges on how rapidly the transplanted (i.e., following radioablation) or remaining (i.e., following chemotherapy) hematopoietic cells can reconstitute the crippled hematopoietic system. The survival rates of recipient mice after either a lethal dose of radiation (12 Gy) or 5-fluorouracil administration were investigated in the presence of either recombinant tPA or a PAI-1 inhibitor. The administration of tPA improved the survival rate after myeloablative treatment, but PAI-1 inhibitor treatment offered significantly more effective protection (Fig. 4A, 4B).

The benefits on the hematopoietic recovery were also confirmed in 9 Gy-irradiated mice, which had been transplanted with BM MNCs. The numbers of both white blood cells and platelets markedly increased after BM transplantation: the PAI-1 inhibitor treatment led to more successful hematopoietic recovery than did the treatment with recombinant tPA (Fig. 4C, 4D). These results demonstrate that the inhibition of PAI-1 promotes hematopoietic recovery and protects against myeloablation-induced mortality.

Suppressing the PAI-1 Activity Induces tPA-Mediated HSC Proliferation in the BM After HSCT

To further elucidate the mechanism(s) by which the PAI-1 inhibition improves the hematopoietic recovery, 2.5×10^6 Ly5.1$^+$ BM cells were transplanted into the 9 Gy-irradiated Ly5.2$^+$ congenic mice, and the effects of tPA or a PAI-1 inhibitor on the proliferation of HSCs were assessed. The absolute number of BM MNCs in the recipients indeed increased in the mice given a PAI-1 inhibitor (Fig. 5A). At 3 weeks after transplantation, both the proportion and the absolute number of phenotypically identified Ly5.1$^+$ donor-derived HSC compartments were significantly higher in the PAI-1 inhibitor-treated mice than in the control or the tPA-treated mice (Fig. 5B–5E). The proportion of mature myeloid and lymphoid Ly5.1$^+$ donor-derived cells in the recipient BM was equivalent in the vehicle-treated and PAI-1 inhibitor-treated recipients, suggesting that the PAI-1 inhibitor does not influence the differentiation of HSCs (Supporting Information Fig. S6). The ability of a PAI-1 inhibitor to induce hematopoietic regeneration, that is, upregulation of MMP and c-kitL production and enhancement of donor cell engraftment was completely negated when the tPA KO mouse was used as the recipient (Fig. 5F–5J), further supporting our hypothesis that the hematopoietic regeneration in our model was derived from the

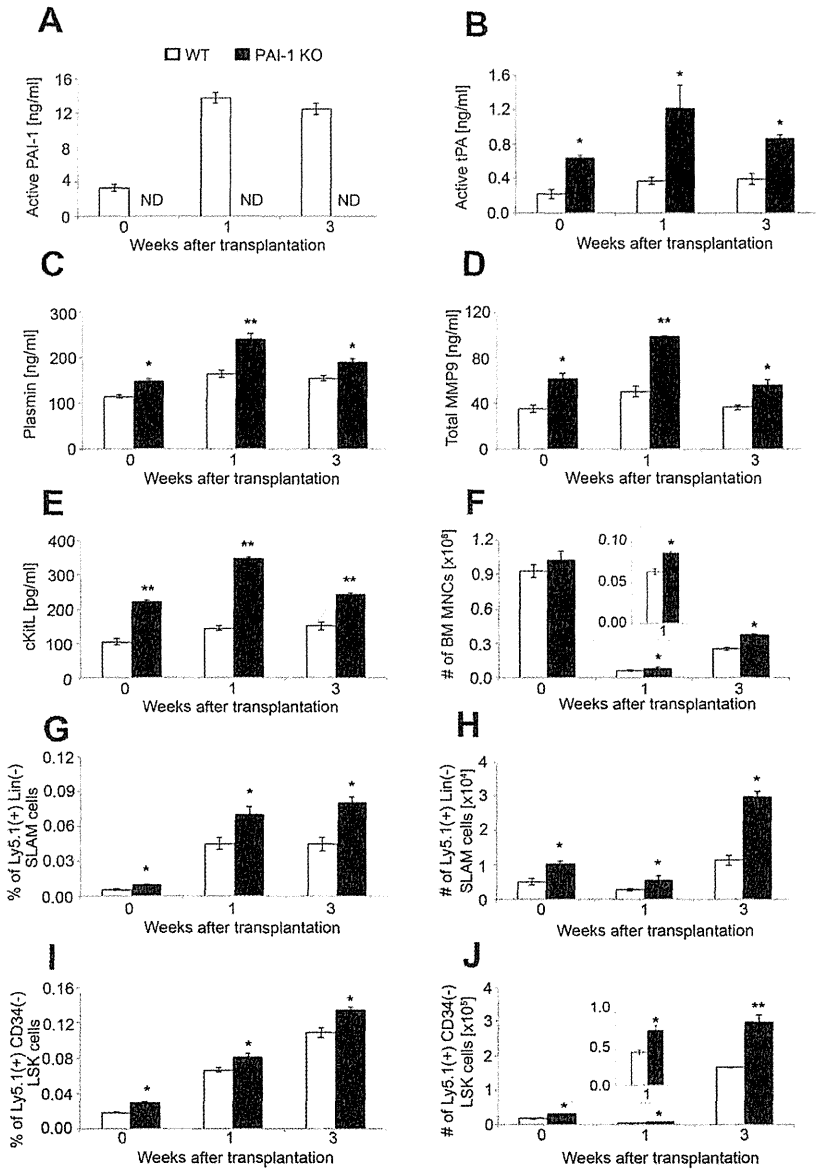

Figure 2. Hematopoietic regeneration is enhanced in PAI-1 KO mice. BM MNCs (2.5×10^6) from the Ly5.1$^+$ donor mice (PAI-1$^{+/+}$) were transplanted into WT (Ly5.2$^+$, PAI-1$^{+/+}$) or PAI-1 KO (Ly5.2$^+$, PAI-1$^{-/-}$) mice that had been irradiated with 9 Gy. Plasma was collected from the recipient mice 1 or 3 weeks after transplantation. **(A–E):** The levels of soluble factors in the plasma. The levels of active PAI-1 (A), active tPA (B), plasmin (C), total MMP-9 (D), and c-kitL (E) in the plasma were determined by enzyme-linked immunoabsorbent assay. Plasma samples from unirradiated (untransplanted) mice were used as controls (0 weeks). White and black bars represent WT and PAI-1KO recipient mice, respectively. The data from three independent experiments are shown ($n = 9$ for each condition). *, $p < .05$; **, $p < .01$ versus WT at the respective time points. ND, not detected. Data are expressed as the means ± SD. **(F–J):** BM MNCs were collected from four long leg bones (two femurs and two tibias) per mouse, pooled, and analyzed by fluorescence-activated cell sorting. The total number of BM MNCs (F), the proportion of Lin$^-$SLAM cells among the donor-derived Ly5.1$^+$ cells (G), the total number of Lin$^-$ SLAM cells (H), the proportion of CD34$^-$LSK cells among Ly5.1$^+$ cells (I), and the total number of CD34$^-$LSK cells (J) were calculated at zero, 1 and 3 weeks. The data from three independent experiments are shown ($n = 9$ for each condition). *, $p < .05$; **, $p < .01$ versus WT at the respective time points. Larger graph scales of the results at 1 week are included as inset graphs in (F) and (J). The data are expressed as the means ± SD. Abbreviations: BM, bone marrow; MNC, mononucleic cell; PAI-1, plasminogen activator inhibitor-1; tPA, tissue-type plasminogen activator; WT, wild type.

PAI-1 inhibition and subsequent tPA-mediated proliferation of HSCs during early hematopoietic reconstitution.

To confirm that the PAI-1 inhibitor induces HSC proliferation, the 9 Gy-irradiated Ly5.2$^+$ congenic mice were transplanted with 2.5×10^6 Ly5.1$^+$ BM cells and given a PAI-1 inhibitor for 5 consecutive days. The expression of Ki67 in the Ly5.1$^+$ donor-derived hematopoietic stem and progenitor cells was examined 1 week after HSCT. The Ki67$^+$ donor-derived LSK

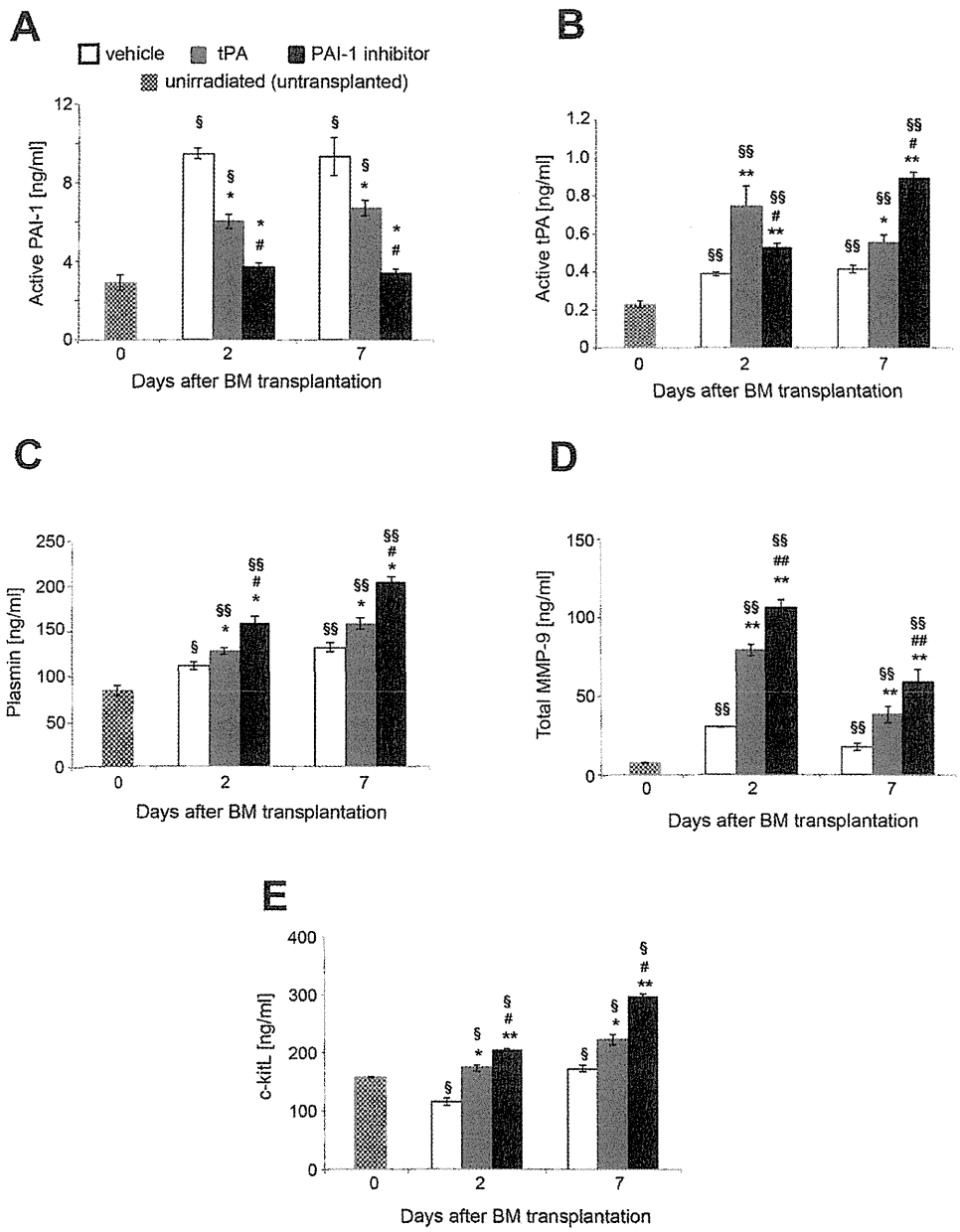

Figure 3. The PAI-1 inhibitor activates the fibrinolytic pathway during hematopoietic regeneration. BM MNCs from the Ly5.1$^+$ donor mice (2.5 $\times$ 10^6) were transplanted into the 9 Gy-irradiated Ly5.2$^+$ mice. Then, vehicle, tPA (10 mg/kg, i.p.), or a PAI-1 inhibitor (TM5275; 100 mg/kg, p.o.) was given daily to the recipient mice for 5 consecutive days. The plasma levels of active PAI-1 **(A)**, active tPA **(B)**, plasmin **(C)**, total MMP-9 **(D)**, and c-kitL **(E)** were measured by enzyme-linked immunoabsorbent assay. The bars in white, gray, and black represent the vehicle-, tPA-, and PAI-1 inhibitor-treated mice, respectively. Hatched bars represent the unirradiated (untransplanted) control mice. The data from four independent experiments are shown as the means $\pm$ SD ($n = 12$ for each condition). *, $p < .05$; **, $p < .01$, versus the vehicle group; $^{\#}$, $p < .05$; $^{\#\#}$, $p < .01$, versus the tPA group; §, $p < .05$; §§, $p < .01$, versus the unirradiated group. Abbreviations: BM, bone marrow; PAI-1, plasminogen activator inhibitor-1; tPA, tissue-type plasminogen activator; MMP-9, matrix metalloproteinase-9.

cells were detected at the highest level in the mice given the PAI-1 inhibitor (Fig. 6A), which correlated with the HSC proportion in the recipient. The inhibition of PAI-1 thus stimulates hematopoietic stem/progenitor cells (HSPCs) to enter into the cell cycle. The PCNA$^+$c-kit$^+$ proliferating HSPCs were preferentially located in the endosteal region of the BM (arbitrarily defined as within 12 cells of the endosteum) [14, 15] at 1 week after transplantation (69.4% $\pm$ 4.1%; $n = 1{,}811$ PCNA$^+$c-kit$^+$ cells in the vehicle-treated group and 76.7% $\pm$ 3.4%; $n = 2{,}983$ PCNA$^+$c-kit$^+$ cells in the PAI-1 inhibitor-treated group, $p < .01$), indicating that the proliferation of HSPCs in the PAI-1 inhibitor-treated recipients as regulated by their interaction with the niche (Fig. 6C).

In the early-stage of regeneration, the HSPCs underwent apoptosis at a higher rate in the vehicle-treated recipient,

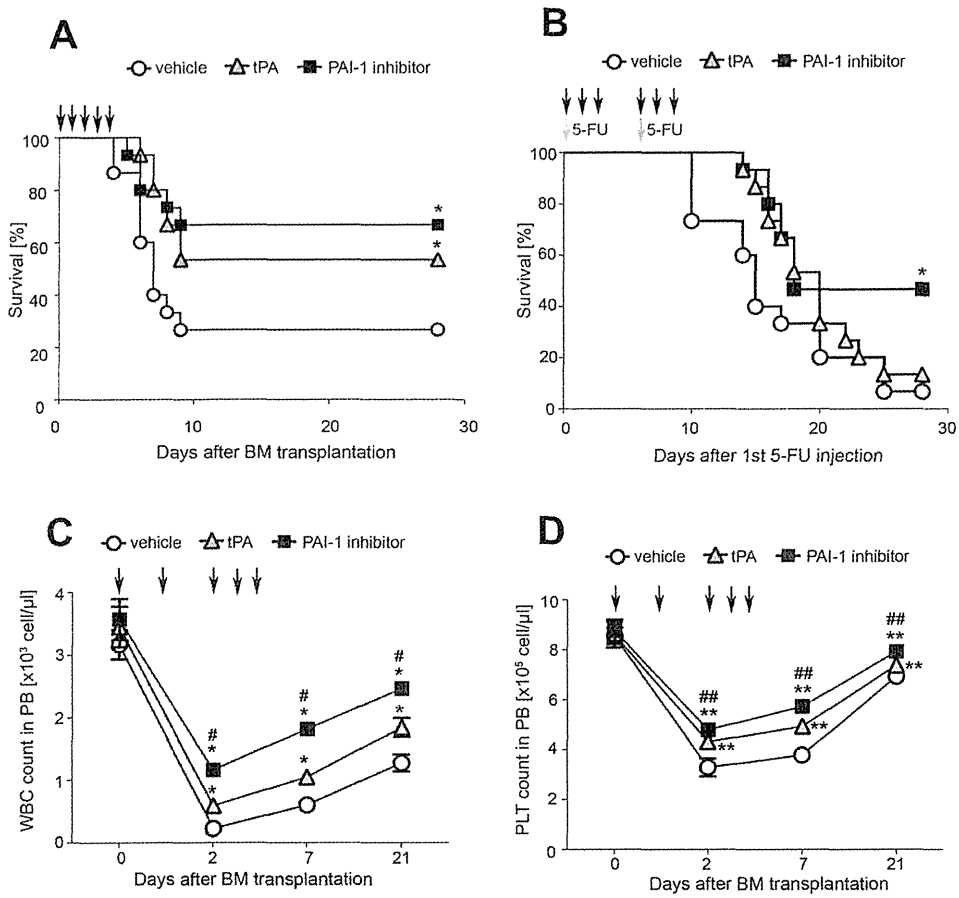

Figure 4. The PAI-1 inhibitor enhances the protection against myeloablation and promotes the rapid recovery of hematopoiesis. **(A):** The survival rate of mice after lethal-dose irradiation. Mice were exposed to 12 Gy of radiation and were transplanted with 1×10^6 BM MNCs. The mice were administered vehicle (white circle), tPA (10 mg/kg, i.p.; gray triangle), or a PAI-1 inhibitor (100 mg/kg, p.o.; black square) daily for 5 consecutive days (arrows). The data from three independent experiments are shown ($n = 15$ for each condition; *, $p < .05$ vs. the vehicle group). **(B):** The survival rate after 5-FU injection. The 5-FU (225 mg/kg, i.p.) was given twice (on days 0 and 7). The mice subsequently received vehicle (white circle), tPA (10 mg/kg, i.p.; gray triangle), or a PAI-1 inhibitor (100 mg/kg, p.o.; black square) for 3 consecutive days after the day of 5-FU injection (arrows). The data from three independent experiments are shown ($n = 15$ for each condition; *, $p < .05$ vs. both the vehicle group and the tPA group). **(C, D):** The hematopoietic recovery. Mice ($Ly5.2^+$) were exposed to 9 Gy of radiation and transplanted with 2.5×10^6 BM MNCs ($Ly5.1^+$). The numbers of white blood cells (WBC, C) and platelets (PLT, D) at the indicated time points were measured. The data from three independent experiments are shown as the means ± SD ($n = 6$ for each condition). *, $p < .05$; **, $p < .01$ versus the vehicle group, #, $p < .05$; ##, $p < .01$ versus the tPA group. Abbreviations: BM, bone marrow; PB, peripheral blood; PAI-1, plasminogen activator inhibitor-1; tPA, tissue-type plasminogen activator; 5-FU, 5-fluorouracil.

whereas the PAI-1 inhibitor prevented the apoptotic cell death of HSPCs (Supporting Information Fig. S7). Altogether, these findings indicate that the PAI-1 inhibitor enhances the proliferation of HSPCs and protects them from stress-induced apoptosis, leading to improve the hematopoietic regeneration.

PAI-1 Inhibition Potentiates the Self-Renewal Capacity of HSCs

The rapid proliferation of HSCs occasionally results in their exhaustion (i.e., loss of competence as HSCs), eventually leading to the failure of long-lasting hematopoiesis in the BM [19–21]. To examine whether the elevation of tPA activity, either by tPA- or PAI-1 inhibitor administration, induced transplanted HSCs to undergo exhaustion, the recipient BM was analyzed at 15 weeks in the $Ly5.2^+$ mice that had been transplanted with $Ly5.1^+$ donor BM cells and given a PAI-1 inhibitor. The results indicated that when the PAI-1 inhibitor was administered to mice, it increased not only the number of BM MNCs (Fig. 7A), but also the proportion, as well as the absolute number of phenotypic $Ly5.1^+$ HSCs compared to the vehicle- or recombinant tPA-treated group (Fig. 7B-7E), suggesting that the inhibition of PAI-1 activity by the PAI-1 inhibitor efficiently prolonged the survival of donor-derived HSCs in the BM.

The self-renewal capacity of HSCs was also examined in a secondary transplant performed 15 weeks after the primary transplant. Twelve weeks after the secondary transplant, the chimerism of the primary donor-derived $Ly5.1^+$ hematopoietic cells was fourfold higher in the PAI-1 inhibitor-treated group than